UKACC International Conference on Control 2012
Cardiff, UK, 3-5 September 2012

State–dependent control of a hydraulically–actuated nuclear decommissioning robot

David Robertson
Engineering Department
Lancaster University, UK
Email: d.robertson@lancaster.ac.uk

C. James Taylor
Engineering Department
Lancaster University, UK
Email: c.taylor@lancaster.ac.uk

***Abstract*—This article develops and evaluates state–dependent parameter (SDP) control systems for the hydraulically actuated dual–manipulators of a mobile nuclear decommissioning robot. A unified framework for calibration, data collection and SDP model identification is proposed, in which the state–dependent variable is a delayed voltage signal associated with the time–varying gain of the system. The latter can cause undesirable joint movements when the device is regulated using linear control algorithms. By contrast, the present article develops a novel nonlinear pole assignment algorithm based on the SDP model. Closed–loop experimental data shows that the SDP design more closely follows the joint angle commands than the equivalent linear algorithm, offering improved resolved motion.**

I. Introduction

The UK nuclear legacy comprises a number of facilities that are significantly contaminated by radioactivity and non–radiological toxins, are sometimes in a relatively poor state of repair and for which knowledge of their use can be incomplete. In fact, the regulatory requirements were very different when first constructed, with the result that many facilities were not designed with decommissioning strategies in mind. In areas of significant contamination, it is necessary to resort to the use of remote and teleoperated mobile robots. These provide an invaluable option for the safe retrieval and disposal of contaminated materials in high–hazard legacy facilities [1].

Mobile robots are used in many hazardous environments, including explosive ordnance disposal, military reconnaissance, natural disaster search and rescue, and in the nuclear decommissioning sector. In the early stages of nuclear clean–up, expensive, bespoke machines were designed, built and commissioned. However, these have suffered from reliability problems and are usually restricted to specific tasks. More recently, off–the–shelf remote solutions are striven for but these lack the ease of control afforded by high–specification bespoke solutions. The research described in this article aims to alleviate this unsatisfactory situation by developing optimized, widely applicable control architectures, that are being tested on an off–the–shelf robotic platform.

The research utilizes a Brokk–40 demolition robot, consisting of a moving vehicle with a single manipulator. Two seven–function HydroLek–HLK–7W robotic arms have been attached to the Brokk, as shown by Fig. 1. Such dual–arm mobile robots now offer a powerful and versatile tool for various types of decommissioning activity [2]. Unfortunately, devices initially developed for heavy lifting are not necessarily suitable for ‘soft touch’ duties such as picking up relatively fragile objects or accurately aligning the end effectors. Indeed, the manipulator can suffer from a relatively slow control action because of limitations in existing linear methods.

Fig. 1. Brokk–40 and dual HydroLek–7W manipulators.

Since the behaviour of hydraulically–driven manipulators is dominated by the nonlinear, lightly–damped dynamics of the actuators, high performance control depends on the introduction of some type of nonlinear model structure. Research embraces approaches such as sliding mode [3], adaptive [4], quasi–linear parameter varying [5] and state–dependent parameter (SDP) design [6], among others. An earlier article considered SDP control of the HydroLek but was limited to simulation and did not consider resolved motion [7].

By contrast, the present article utilises open and closed–loop experimental data to investigate potential state dependencies and resolved motion. Here, the nonlinear system is modelled using the quasi–linear SDP structure [8]. For the HydroLek, a novel non–minimal state variable feedback ‘regulator’ is adapted from the nonlinear pole assignment algorithm of [9]. The data collection and kinematics are described in sections II and III, followed in section IV by an overview of the control design method. Finally, the experimental results and conclusions are discussed in sections V and VI.

978-1-4673-1558-6/12/$31.00 ©2012 IEEE

II. Mobile Robot Platform

The hardware arrangement was developed at Lancaster University from components supplied by Brokk UK Ltd and HydroLek Ltd [2]. The Brokk–40 base machine is 650mm wide, allowing for access through narrow doorways. The five Degrees–Of–Freedom (DOF) manipulator is usually equipped with a variety of tools, including percussive breakers, hydraulic crushing jaws, excavating buckets and concrete milling heads. The unit is electrically powered to facilitate internal use, with an onboard hydraulic pump to power the caterpillar tracks and, by means of several hydraulic pistons, the manipulator.

For decommissioning tasks, accessing the robot on–site to change tools could be a slow, laborious and potentially hazardous task. A more flexible system with the ability to perform multiple tasks without a tool change has been achieved with the mounting of two HydroLek–HLK–7W, seven DOF manipulators, each consisting of six rotational joints and a gripper. The combined system is shown in Fig. 1, whilst Fig. 2 illustrates the azimuth yaw, shoulder pitch, elbow pitch, forearm roll and wrist pitch joints. These are fitted with potentiometer feedback sensors, allowing the position of the end–effector to be determined during operation. The joints are actuated via hydraulic pistons, which are powered via an auxiliary output from the hydraulic pump of the Brokk unit.

A standard input device, such as a joystick, is connected to a PC running a graphical user interface developed for the NI Labview software environment. The PC transmits information to a NI Compact Fieldpoint Real–Time controller (cFP) via an Ethernet networking connection. The cFP is a stand alone device running a real–time operating system, allowing for the precise sampling rates needed for discrete–time control. The hydraulic pistons are controlled by seven pairs of control valves, where each pair has an input for both positive and negative flow. Output modules convert the digital cFP signal to a varied voltage fed to the control valves.

The present authors have developed a semi–automated system for calibrating and initialising the robot for open–loop data collection [10]. Here, the robot is manipulated into a suitable configuration using 'de–tuned' proportional control systems. The operator selects from classical step experiments or pseudo–random signals for the estimation of nonlinear models. Figure 3 summarises the basic control system for a single joint. The system input u_k is scaled to lie in the range -100, representing the maximum power in a negative 'closing' direction, through to +100, representing the maximum power in a positive 'opening' direction. The dead–band of the system is eliminated by the input calibration step, hence an input of zero represents no movement. The output y_k is the potentiometer voltage, representing a scaled joint angle.

III. Inverse Kinematics

Since it has no bearing on the end–effector location, the gripper is neglected from the kinematic solution illustrated in Figure 4. Gripper control will be considered separately on the basis of pressure feedback and is beyond the scope of the present article. Hence, each manipulator is described as

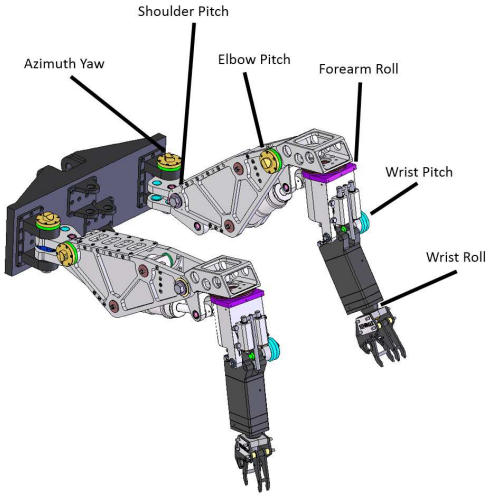

Fig. 2. HydroLek–7W rotational joints.

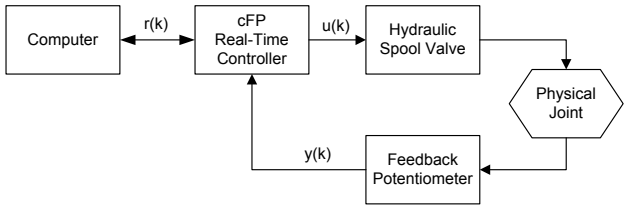

Fig. 3. Control system overview for a single joint.

a kinematic model with six solid links and rotational joints. In fact, the manipulator is over–specified in terms of end–effector positioning, with the additional degrees–of–freedom potentially utilised to allow the end–effectors orientation to be set and to reach past obstacles (for example, to pick up a contaminated object from a container/skip). The system is non–trivial to solve for a closed–form, hence incremental steps in complexity are utilised for testing control performance.

The present research concentrates on the development of novel joint control systems and initially evaluates these using a reduced 2–DoF system that allows for straightforward movement of the end–effector in a plane. Figure 5 shows how the manipulator is limited to a straightforward 2–DoF system for Joints 2 and 3, with the remaining joints locked off. Equations (1) and (2) describe the forward kinematic relationship of P_x and P_z to the joint angles θ_1 and θ_2, for a generic 2–DoF planer robot, where P_x and P_z represent the horizontal and vertical positions of the end–effector respectively.

$$P_x = l_2 c_{12} + l_1 c_1 \tag{1}$$

$$P_z = l_2 s_{12} + l_1 s_1 \tag{2}$$

Here, c_1 and s_1 denote $\cos(\theta_1)$ and $\sin(\theta_1)$ respectively, c_{12} and s_{12} represent $\cos(\theta_1 + \theta_2)$ and $\sin(\theta_1 + \theta_2)$, while l_1 and l_2 are link lengths. Equations (3) and (4) show how this description is applied to the manipulator geometry in Figure 5,

$$P_x = R c_{23-r} + a_2 c_2 + a_1 \tag{3}$$

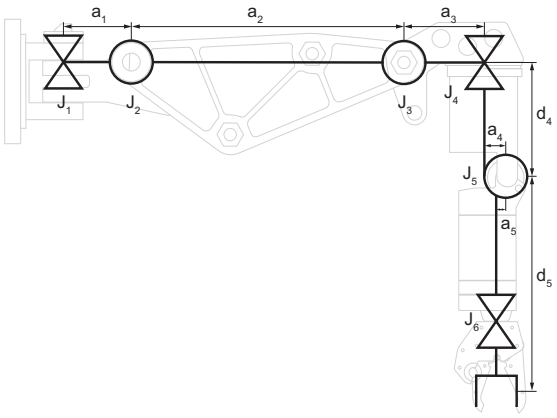

Fig. 4. 6–DOF kinematic description of HydroLek–7W Manipulator.

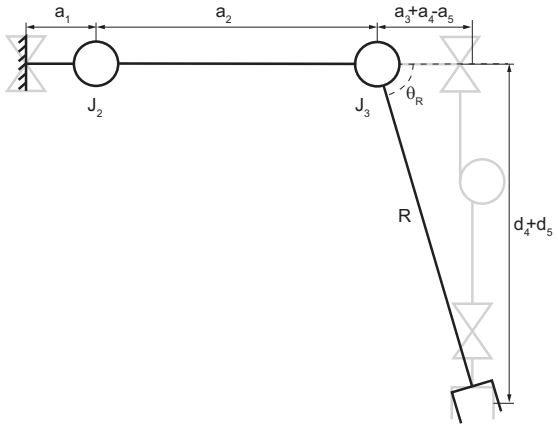

Fig. 5. 2–DOF description of HydroLek–7W Manipulator.

$$P_z = Rs_{23-r} + a_2 s_2 \tag{4}$$

in which θ_2 and θ_3 represent the shoulder pitch and elbow pitch respectively (Figure 2), $\theta_R = \text{atan2}(a_3{+}a_4{-}a_5, d_4{+}d_5)$, $R = \sqrt{(a_3+a_4-a_5)^2+(d_4+d_5)^2}$ and c_{23-r} represents $\cos(\theta_2+\theta_3-\theta_R)$. The inverse kinematics are subsequently derived as follows [11],

$$c_3 = \frac{(P_x-a_1)^2 + P_z^2 - R^2 - a_2^2}{2a_2R} \tag{5}$$

$$s_3 = \pm\sqrt{1-c_3^2} \tag{6}$$

$$\theta_3 = \text{atan2}\,(s_3, c_3) + \theta_R \tag{7}$$

Similarly,

$$c_2 = \frac{(P_x-a_1)(Rc_3+a_2) + P_zRs_3}{d} \tag{8}$$

$$s_2 = \frac{P_z(Rc_3+a_2) - (P_x-a_1)Rs_3}{d} \tag{9}$$

where $d = (Rc_3+a_2)^2 + (Rs_3)^2$. Hence, θ_2 is solved by,

$$\theta_2 = \text{atan2}\,(s_2, c_2) \tag{10}$$

IV. Nonlinear pole assignment

Consider the deterministic form of the SDP model:

$$y_k = \mathbf{w}_k^{\mathrm{T}}\mathbf{p}_k \tag{11}$$

where $\mathbf{w}_k^{\mathrm{T}}$ is a vector of lagged input and output variables and $\mathbf{p}_k$ is a vector of SDP parameters, defined as follows,

$$\mathbf{w}_k^{\mathrm{T}} = \begin{bmatrix} -y_{k-1} & \cdots & -y_{k-n} & u_{k-1} & \cdots & u_{k-m} \end{bmatrix}$$
$$\mathbf{p}_k = \begin{bmatrix} a_1\{\boldsymbol{\chi}_k\} & \cdots & a_n\{\boldsymbol{\chi}_k\} & b_1\{\boldsymbol{\chi}_k\} & \cdots & b_m\{\boldsymbol{\chi}_k\} \end{bmatrix}^{\mathrm{T}}$$

Here y_k is the output and u_k the control input, while $a_i\{\boldsymbol{\chi}_k\}\,(i=1,2,\ldots,n)$ and $b_j\{\boldsymbol{\chi}_k\}\,(j=1,\ldots,m)$ are n and m state dependent parameters. The latter are assumed to be functions of a non–minimal state vector,

$$\boldsymbol{\chi}_k^{\mathrm{T}} = \begin{bmatrix} \mathbf{w}_k^{\mathrm{T}} & \mathbf{U}_k^{\mathrm{T}} \end{bmatrix} \tag{12}$$

in which $\mathbf{U}_k = [U_{1,k}, U_{2,k}, \ldots, U_{r,k}]$ is a vector of measured variables, potentially including other joint angles. Any pure time delay $\tau \geq 1$ is represented by setting the leading $b_1\{\boldsymbol{\chi}_k\}\ldots b_{\tau-1}\{\boldsymbol{\chi}_k\}$ terms to zero. To identify and estimate this model from experimental data, the authors have used the back–fitting approach of references [8] and [12].

Using this model, the first author and colleagues have developed a novel method for nonlinear pole assignment of SDP systems that guarantees closed–loop stability at the design stage: see references [6] and [9] for details. The approach is based on the definition of a suitable non–minimal state space (NMSS) form. For the present research, the algorithm has been modified to handle the integrating joint angle dynamics. In particular, the dead–zone calibration routine ensures that there is no movement when $u_k = 0$, hence external integral action is not required. In fact, the destabilizing nature of integral action has a negative impact on the control performance. For this reason, the following 'regulator' NMSS form is utilised:

$$\mathbf{x}_{k+1} = \mathbf{F}\{\boldsymbol{\chi}_k\}\,\mathbf{x}_k + \mathbf{g}u_k \quad ; \quad y_k = \mathbf{h}\mathbf{x}_k \tag{13}$$

where the $n+m-1$ dimensional state vector is,

$$\mathbf{x}_k = \begin{bmatrix} y_k & \cdots & y_{k-n+1} & u_{k-1} & \cdots & u_{k-m+1} \end{bmatrix}^T \tag{14}$$

and the state matrices are defined to satisfy the SDP model (11), as shown by the example in section V. The state variable feedback control algorithm is,

$$u_k = -\mathbf{v}\{\boldsymbol{\chi}_k\}\,\mathbf{x}_k + k_0\{\boldsymbol{\chi}_k\}\,r_k \tag{15}$$

where,

$$\mathbf{v}\{\boldsymbol{\chi}_k\} = [f_0\{\boldsymbol{\chi}_k\}\ldots f_{n-1}\{\boldsymbol{\chi}_k\}\,g_1\{\boldsymbol{\chi}_k\}\ldots g_{m-1}\{\boldsymbol{\chi}_k\}]$$

is a vector of scheduled control gains, r_k is the command input and $k_0\{\boldsymbol{\chi}_k\} = f_0\{\boldsymbol{\chi}_k\} + \ldots + f_{n-1}\{\boldsymbol{\chi}_k\}$. A vector $\mathbf{c}\{\boldsymbol{\chi}_k\}$ is defined with a similar structure to $\mathbf{v}\{\boldsymbol{\chi}_k\}$ but in which $\bar{g}_i\{\boldsymbol{\chi}_k\}\,(i=1\ldots m-1)$ differ from $g_i\{\boldsymbol{\chi}_k\}$ as follows,

$$g_i\{\boldsymbol{\chi}_k\} = \frac{b_\tau\{\boldsymbol{\chi}_{k+\tau-i}\}}{b_\tau\{\boldsymbol{\chi}_{k+\tau}\}} \cdot \bar{g}_i\{\boldsymbol{\chi}_k\} \tag{16}$$

Here, $\mathbf{c}\{\boldsymbol{\chi}_k\}$ is determined by defining a suitable matrix $\Sigma_k\{\boldsymbol{\chi}_k\}$ of model coefficients and solving,

$$\Sigma\{\boldsymbol{\chi}_k\} \cdot \mathbf{c}\{\boldsymbol{\chi}_k\} = \mathbf{d} - \mathbf{p}\{\boldsymbol{\chi}_k\} \quad (17)$$

in which $\mathbf{p}\{\boldsymbol{\chi}_k\}$ and $\mathbf{d}$ are the open–loop and desired (time–invariant and stable) closed–loop coefficients respectively [6]. For brevity, full definitions of the above matrices are omitted but illustrative solutions for the HydroLek manipulator are presented in section V. The scaling (16) is necessary in order to achieve the desired stable closed–loop response and imposes a clear limitation on $b_\tau\{\boldsymbol{\chi}_{k+\tau}\}$. In fact, $b_\tau\{\boldsymbol{\chi}_{k+\tau}\} \neq 0$ corresponds directly to the pole assignability condition [6].

V. Results

Preliminary open–loop step experiments (not shown) suggest that a first order linear difference equation, i.e.,

$$y_k = -a_1 y_{k-1} + b_\tau u_{k-\tau} \quad (18)$$

provides an approximate representation of individual joints, with time–invariant parameters $\{a_1, b_\tau\}$ and the time delay τ depending on the sampling interval Δt. Such models have previously been utilized for the development of linear control systems for large scale hydraulic machinery in the construction industry [13]. However, further analysis quickly reveals limitations in the linear model. For the HydroLek, it is readily apparent that the numerical values of $\{a_1, b_\tau\}$ are not repeatable for different step experiments. Most notably, the value of b_τ depends on the magnitude of the applied voltage utilized for these step experiments, i.e. it is a SDP.

A. System identification

Various candidate SDP structures have been investigated for open–loop movement of the right hand side manipulator shoulder and elbow pitch, moving in air with no additional loading terms, i.e. no objects are held by the gripper. For these conditions, trial and error experimentation suggests that a sampling interval of $\Delta t = 0.07$ seconds yields a satisfactory compromise between a fast response and the following low–order model for control system design,

$$y_k = -a_1\{y_{k-1}\}\, y_{k-1} + b_2\{u_{k-2}\}\, u_{k-2} \quad (19)$$

The model is based on equation (11) with $n = 1$, $m = \tau = 2$, $b_1\{\boldsymbol{\chi}_k\} = 0$ and initially $\boldsymbol{\chi}_k = [y_{k-1} u_{k-2}]$. In fact, the statistical estimates suggest that $a_1\{\boldsymbol{\chi}_k\}$ is relatively constant over time, with the pole close to unity. Assuming $a_1 = -1$, the system essentially behaves as an integrator. In this case, $b_2\{\boldsymbol{\chi}_k\}$ represents the state–dependent angular velocity, approximated by the following second order polynomial,

$$b_2\{u_{k-2}\} = p_1 u_{k-2}^2 + p_2 u_{k-2} + p_3 \quad (20)$$

The coefficients in equation (20) are optimized from open–loop experiments using fminsearch in Matlab®, yielding the estimates shown in Table I. The model responses (18) and (19) are compared with measured data for an illustrative open–loop shoulder joint experiment in Fig. 6. The SDP model is far superior, typically explaining over 95% of the output variance, compared with only 20–60% for the linear model.

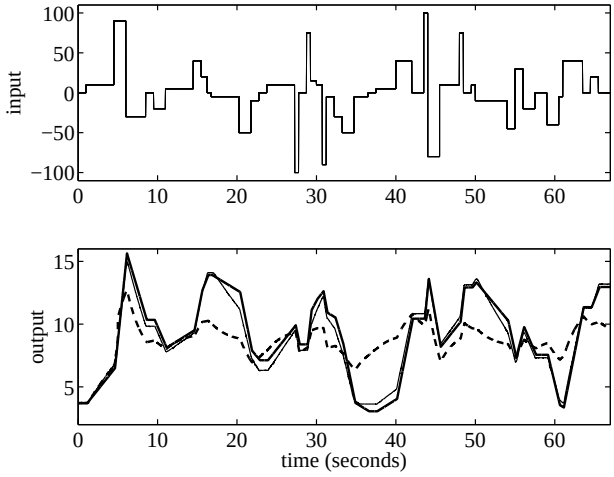

Fig. 6. Upper subplot: applied input voltage plotted against time. Lower subplot: potentiometer voltage, showing the optimized SDP model response (thick trace), experimental data (thin) and linear model (dashed).

TABLE I
Optimized polynomial coefficients

Joint	p_1	p_2	p_3
θ_2	$-2.2898e^{-007}$	$1.2576e^{-005}$	0.0055
θ_3	$-1.9290e^{-007}$	$1.8214e^{-005}$	0.0051

B. Control system design

The NMSS/SDP (13) representation of equation (19) is,

$$\mathbf{x}_k = \begin{bmatrix} y_k \\ u_{k-1} \end{bmatrix} = \begin{bmatrix} -a_1 & b_2\{u_{k-2}\} \\ 0 & 0 \end{bmatrix} \mathbf{x}_{k-1} + \begin{bmatrix} 0 \\ 1 \end{bmatrix} u_{k-1} \quad (21)$$

and $y_k = \begin{bmatrix} 1 & 0 \end{bmatrix} \mathbf{x}_k$. For $b_2\{u_{k-2}\} > 0$, the matrix $\Sigma\{\boldsymbol{\chi}_k\}$ in equation (17) can always be inverted, i.e.,

$$\begin{bmatrix} f_0\{\boldsymbol{\chi}_k\} \\ \bar{g}_1 \end{bmatrix} = \begin{bmatrix} 0 & 1 \\ b_2\{u_{k-2}\} & a_1 \end{bmatrix}^{-1} \begin{bmatrix} -p_1 - p_2 - a_1 \\ p_1 p_2 \end{bmatrix} \quad (22)$$

in which $(z - p_1)(z - p_2) = z^2 - (p_1 + p_2) z + p_1 p_2$ is the desired closed–loop characteristic polynomial, with the poles $\{p_1, p_2\}$ chosen to lie within the unit circle of the complex z–plane. For the illustrative results considered in Figures 7, 8 and 9, $p_1 = 0.9$ and $p_2 = 0.94$ are chosen by trial and error simulation. Utilising (16), the control algorithm (15) is,

$$u_k = -f_0\{\boldsymbol{\chi}_k\}\, y_k - \frac{b_2\{u_{k-2}\}}{b_2\{u_{k-1}\}} g_1 u_{k-1} + k_0\{\boldsymbol{\chi}_k\}\, r_k \quad (23)$$

where $f_0\{\boldsymbol{\chi}_k\} = k_0\{\boldsymbol{\chi}_k\} = (p_1 p_2 - g_1)/b_2\{u_{k-2}\}$ and $g_1 = -p_1 - p_2 - a_1$. Note that g_1 is time–invariant in this case. For the HydroLek, $a_1 = -1$ and $b_2\{u_{k-2}\}$ is defined by equation (20). Finally, three linear control systems are also considered. Experimental results suggests that the most robust linear algorithm is based on an operating level of $u_k = 0$, hence utilising equation (20) and Table I, $b_2 = 0.0055$ and $b_2 = 0.0051$ for the shoulder and elbow joints respectively. For comparison, linear controllers are also developed for the maximum input signal each direction, i.e. equation (20) with $u_k = -100$ and $u_k = 100$. In each case, equation (22) is solved off–line for these time–invariant coefficients.

C. Experimental results

Typical practical results for the NMSS/SDP controller are illustrated by Fig. 7, showing a satisfactory response across a range of operating levels. The linear controller based on an operating level of $u_k = 0$ or 100 yields a slower response (not shown), since the model utilised tends to 'overestimate' the steady state gain of the system. By contrast, the linear controller based on $u_k = -100$ works adequately for large negative steps in the command (since these are associated with large negative values of the input) but tends to overshoot the set point at other times, as illustrated by Fig. 8.

Here, it should be emphasized that the control objective is to follow the particular response specified by the design poles. Although arbitrarily chosen for the present article, which focuses on the low–level joint control problem, the poles and command sequences are generally determined by the higher–level control module for optimising tasks using the attached tools. Hence, the faster speed of response and overshoot for the linear design in Fig. 8 represents an undesirable deviation from the required behaviour of the system.

Fig. 9 shows this error between the experimentally observed joint angle and the ideal or 'design' response. The latter is obtained by simulating a transfer function with the design poles in open–loop. In Fig. 9, the grey and black shading highlights the errors for the SDP and linear controllers respectively. Hence the black colour represents the *additional* errors associated with the linear controller in each case, demonstrating the improved performance of the NMSS/SDP design against all three linear controllers. The mean absolute errors between the joint angle and ideal response for each of the controllers (i.e. SDP and the linear controllers associated with each operating level) are summarised in Table II, for experiments similar to Fig. 7 and Fig. 8.

Finally, Figures 10 and 11 illustrate a resolved motion experiment based on the kinematic equations discussed in section III. Here, the end–effector is programmed to trace a circle in a clockwise motion, followed by a second lower circle in an anticlockwise direction, with point–to–point motion between. In fact, the circular movement is also based on point–to–point motion, with the trajectory defined by a series of small steps in the positional set point for $[p_x, p_z]$. The speed of response is determined by the number of iterations and the waiting time for each point. This straightforward approach to positional trajectory planning appears to work well in practice for hydraulically operated robotic manipulators [13].

Although the linear and nonlinear responses in Figure 10 are visually very similar, small joint angle errors are propagated in relation to the position of the end–effector for these resolved motion experiments. Once the experimental data are displayed in Cartesian form on the work–plane, as in Figure 11, the potential benefits of high performance nonlinear control become more apparent, particularly when relatively fast movement is required. For the illustrative results shown, each circle was programmed to be completed in 6 seconds, with the experiment repeated three times in Figure 11.

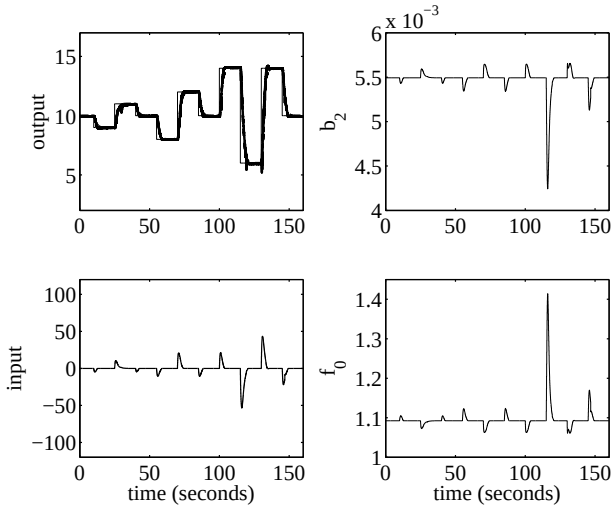

Fig. 7. Clockwise from upper left: closed–loop experiment showing the response of joint angle (thick trace) to a sequence of step changes in the command (thin), $b_2\{\boldsymbol{\chi}_k\}$, $f_0\{\boldsymbol{\chi}_k\}$ and u_k, all plotted against time.

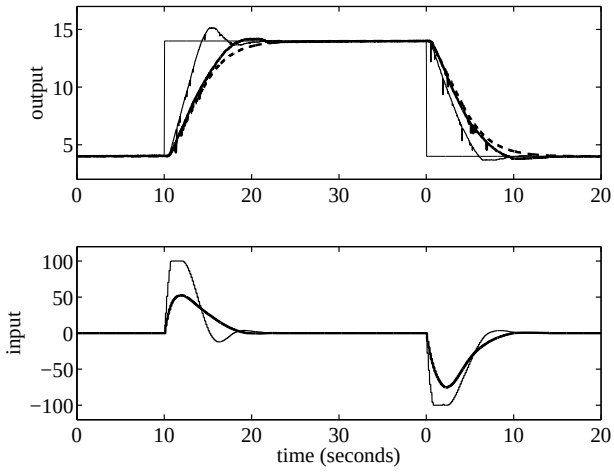

Fig. 8. Closed–loop response of joint angle to positive (joint opening) and negative (closing) step changes in the command input, showing experimental data obtained using the linear (thin trace) and nonlinear (thick) controllers, compared to the simulated design response (dashed), all plotted against time. Upper subplot: potentiometer voltage. Lower subplot: applied input voltage.

VI. Conclusions

This article has considered state–dependent parameter (SDP) models and non–minimal state space (NMSS) control design for the hydraulically actuated joints of a mobile robot designed for nuclear decommissioning. The analysis suggests that a univariate SDP model with state–dependent gain, representing the angular velocity, is adequate for fast and smooth control of the manipulators. However, the authors are presently investigating other configurations and settings with a view to identifying additional state variables and potential multivariable state–dependencies.

To illustrate the modelling approach and typical closed–loop results, the analysis has concentrated on experimental data associated with the shoulder and elbow pitch of one

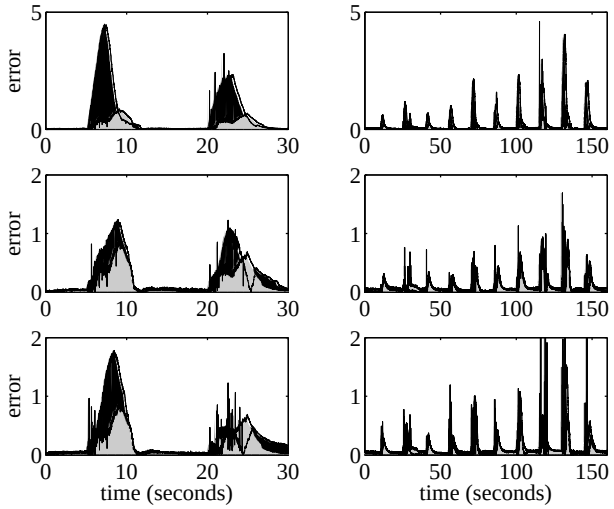

Fig. 9. Errors between the experimentally observed joint angle and the design response, plotted against time, comparing the nonlinear (grey shading) and linear (black) controllers for experiments similar to Fig. 7 (right hand side subplots) and Fig. 8 (left). Upper subplots: linear controller based on operating level $u_k = -100$. Middle subplots: $u_k = 0$. Lower subplots: $u_k = 100$.

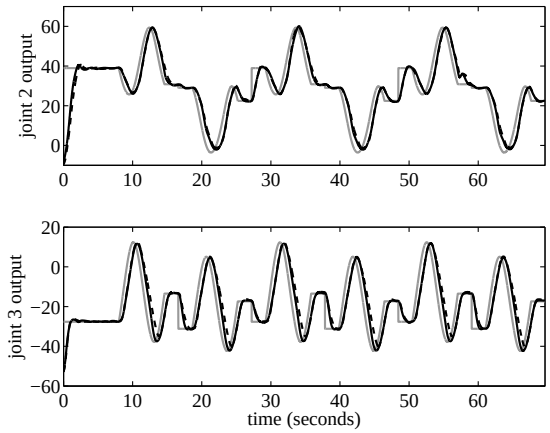

Fig. 10. Closed–loop response for a resolved trajectory, showing experimental data obtained using the linear (dashed) and nonlinear (black) controllers, together with the set point generated by the inverse kinematics (gray), plotted against sample number. Upper subplot: Joint 2. Lower subplot: Joint 3.

manipulator. The authors are now investigating the remaining joints, with a view to the development of a high–level control algorithm for resolved control of the dual–manipulators. In the future, these algorithms are intended to be part of a self–calibrating and self–tuning automatic control system.

ACKNOWLEDGMENT

The authors are grateful for the support of Brokk UK Ltd. and HydroLek Ltd., who supplied the base robotic systems, and the Nuclear Decommissioning Authority (NDA), who have part–funded this research. The statistical tools have been assembled as the CAPTAIN toolbox within the Matlab® software environment and may be obtained from the second author [12].

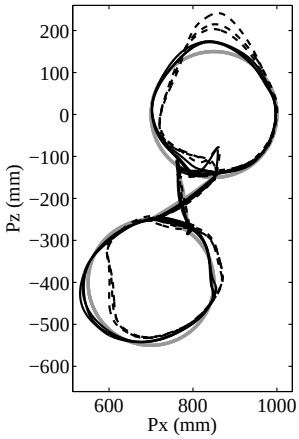

Fig. 11. End–effector location associated with Fig. 10, showing experimental data obtained using the linear (dashed) and nonlinear (black) controllers, together with the set point generated by the inverse kinematics (gray).

TABLE II
MEAN ABSOLUTE ERROR BETWEEN JOINT ANGLE AND IDEAL RESPONSE.

	SDP	$u_k = -100$	$u_k = 0$	$u_k = 100$
Fig. 7	0.1640	0.5229	0.2414	0.2400
Fig. 8	0.0921	0.2289	0.1030	0.1346

REFERENCES

[1] D. W. Seward, C. M. Pace, and R. Agate, "Safe and effective navigation of autonomous robots in hazardous environments," *Journal of Autonomous Robots*, vol. 22, pp. 223–242, 1999.
[2] M. J. Bakari, D. W. Seward, and C. J. Taylor, "The development of a prototype of a multi–arm robotic system for decontamination and decommissioning applications within the nuclear industry," in *12th International Conference on Environmental Remediation and Radioactive Waste Management*, Liverpool, UK, October 2009.
[3] Q. Ha, D. Rye, and H. Durrant-Whyte, "Fuzzy moving sliding mode control with application to robotic manipulators," *Automatica*, vol. 35, pp. 607–616, 1999.
[4] M.-H. Chiang and H. Murrenhoff, *Adaptive servo–control for hydraulic excavators*, ser. Power Transmission and Motion Control. Professional Engineering Publishing Limited, UK, 1998.
[5] B. Fidan, Y. Zhang, and P. A. Ioannou, "Adaptive control of a class of slowly time varying systems with modeling uncertainties," *IEEE Transactions on Automatic Control*, vol. 50, pp. 915–920, 2005.
[6] C. J. Taylor, A. Chotai, and P. C. Young, "Nonlinear control by input–output state variable feedback pole assignment," *International Journal of Control*, vol. 82, pp. 1029–1044, 2009.
[7] C. J. Taylor, A. Chotai, and D. Robertson, "State dependent control of a robotic manipulator used for nuclear decommissioning activities," in *IEEE International Conference on Intelligent Robots and Systems (IROS)*, Taipei, Taiwan, October 2010.
[8] P. C. Young, P. McKenna, and J. Bruun, "Identification of nonlinear stochastic systems by state dependent parameter estimation," *International Journal of Control*, vol. 74, pp. 1837–1857, 2001.
[9] C. J. Taylor, A. Chotai, and K. J. Burnham, "Controllable forms for stabilising pole assignment design of generalised bilinear systems," *Electronics Letters*, vol. 47, pp. 437–439, 2011.
[10] D. Robertson, "HydroLek data acquisition & controller testing," Engineering Department, Lancaster University, UK, Tech. Rep., 2011.
[11] R. Manseur, *Robot Modelling & Kinematics*. Charles River, 2006.
[12] C. J. Taylor, D. J. Pedregal, P. C. Young, and W. Tych, "Environmental time series analysis and forecasting with the Captain Toolbox," *Environmental Modelling and Software*, vol. 22, no. 6, pp. 797–814, 2007.
[13] E. M. Shaban, S. Ako, C. J. Taylor, and D. W. Seward, "Development of an automated verticality alignment system for a vibro–lance," *Automation in Construction*, vol. 17, pp. 645–655, 2008.